Idealized Model Simulations Examining the Mesoscale Structure of Winter Lake-Effect Circulations

NEIL F. LAIRD

Department of Atmospheric Sciences, University of Illinois at Urbana–Champaign, Urbana, Illinois, and Geoscience Department, Hobart and William Smith Colleges, Geneva, New York

DAVID A. R. KRISTOVICH

Atmospheric Environment Section, Illinois State Water Survey, Illinois Department of Natural Resources, Champaign, Illinois, and Department of Atmospheric Sciences, University of Illinois at Urbana–Champaign, Urbana, Illinois

JOHN E. WALSH

Department of Atmospheric Sciences, University of Illinois at Urbana–Champaign, Urbana, Illinois

(Manuscript received 2 May 2001, in final form 22 June 2002)

ABSTRACT

An array of 35 idealized mesoscale model simulations was used to examine environmental and surface forcing factors controlling the meso-β-scale circulation structure resulting from cold flow over an isolated axisymmetric body of water at the midlatitudes. Wind speed, lake–air temperature difference, ambient atmospheric stability, and fetch distance were varied across previously observed ranges. Simulated meso-β-scale lake-effect circulations occurred within three basic regimes (e.g., vortices, shoreline bands, widespread coverage), similar to observed morphological regimes. The current study found that the morphological regimes of lake-effect circulations can be predicted using the ratio of wind speed to maximum fetch distance (U/L). Lake-effect environmental conditions producing low values of U/L (i.e., approximately < 0.02 m s^{-1} km^{-1}) resulted in a mesoscale vortex circulation. Conditions leading to U/L values between about 0.02 and 0.09 m s^{-1} km^{-1} resulted in the development of a shoreline band, and U/L values greater than approximately 0.09 m s^{-1} km^{-1} produced a widespread coverage event. It was found that transitions from one morphological regime to another are continuous and within transitional zones the structure of a circulation may contain structural features characteristic of more than one regime. Results show that 1) the U/L criterion effectively classifies the morphology independently of the lake–air temperature difference for the parameter value combinations examined and 2) the Froude number, suggested as a potential lake-effect forecasting tool in previous studies, does not permit the unique classification of lake-effect morphology.

1. Introduction

A fundamental outstanding issue in mesoscale and boundary layer research is how the atmosphere responds to, and interacts with, surface heat and moisture variations. The development of mesoscale circulations is often associated with spatial heterogeneities in surface heat fluxes. These surface heterogeneities can result from land–water boundaries, surface vegetation and land use differences, sea surface temperature gradients, polar sea ice openings, and soil wetness variations (e.g., Segal and Arritt 1992). Excellent examples of the development of mesoscale circulations in response to variations in surface heat fluxes are lake-effect winter storms. These mesoscale systems are closely coupled to their surface heat and moisture source (i.e., lake) and therefore often result in significant localized snowfall near the lakeshores.

Meso-β-scale (i.e., 20–200 km) circulations that develop during the late fall and winter in response to cold air flow over open lake waters, such as the Great Lakes, can often be characterized by a distinct morphological regime (Braham and Kelly 1982; Hjelmfelt 1990; Niziol et al. 1995). The four most commonly discussed regimes include 1) widespread coverage (e.g., Kelly 1986; Kristovich and Laird 1998), 2) shoreline bands (e.g., Hjelmfelt and Braham 1983), 3) midlake bands (e.g., Passarelli and Braham 1981), and 4) mesoscale vortices (e.g., Forbes and Merrit 1984; Pease et al. 1988; Laird 1999). For purposes of this investigation, shoreline and midlake bands are consolidated into a single morphological re-

Corresponding author address: Neil F. Laird, Dept. of Atmospheric Sciences, University of Illinois at Urbana–Champaign, 105 S. Gregory St., Urbana, IL 61801.
E-mail: n-laird@uiuc.edu

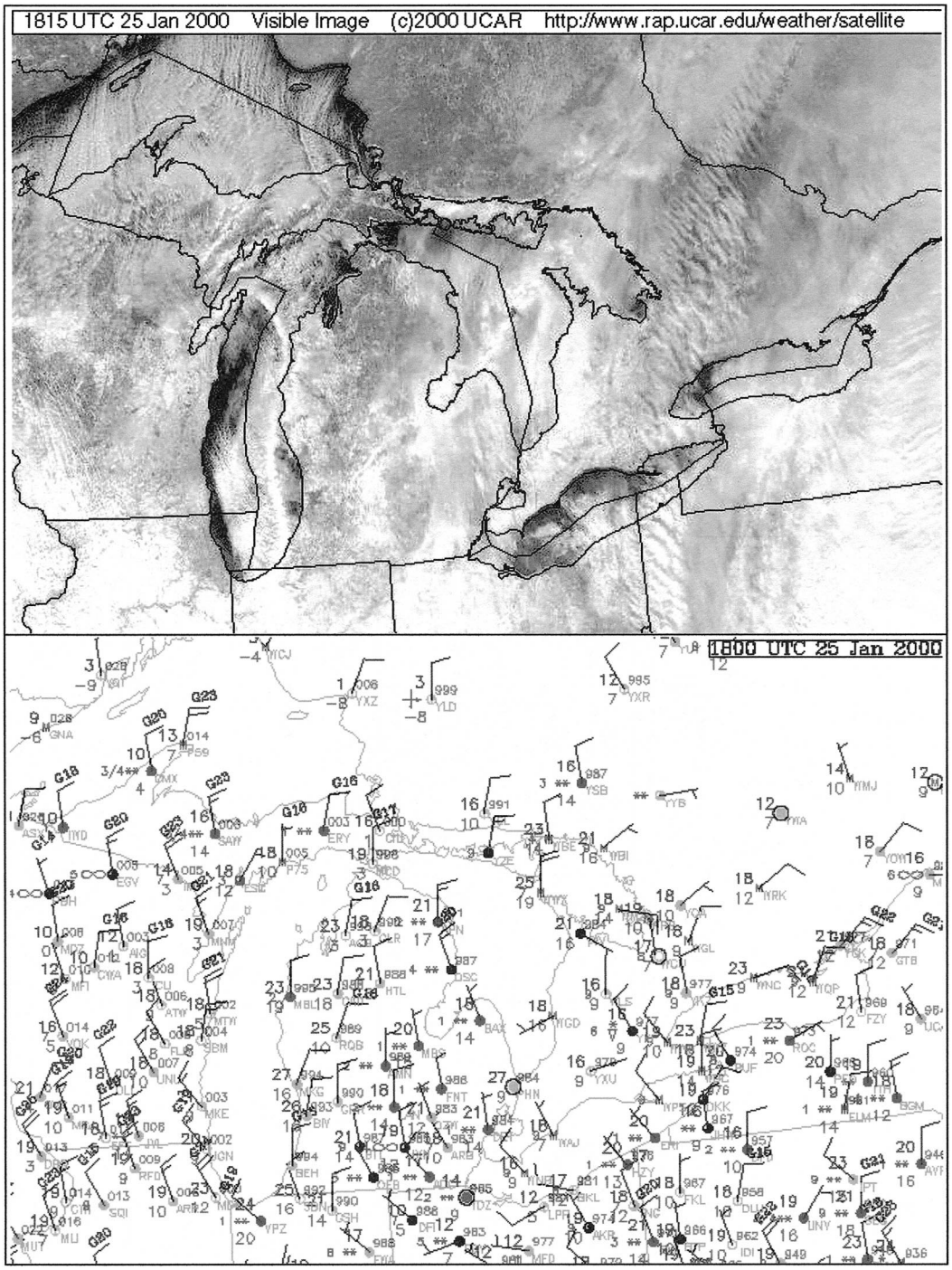

FIG. 1. Typical mesoscale lake-effect structures. (top) Geostationary Operational Environmental Satellite (GOES) visible image at 1815 UTC 25 Jan 2000 of a mesoscale vortex, shoreline band, and widespread coverage event over Lakes Huron, Michigan, and Superior, respectively. (bottom) Corresponding Great Lakes region standard surface analysis at 1800 UTC.

gime called shoreline bands, since conditions used to distinguish these two types of lake-effect bands can often occur simultaneously.

An example of the three primary lake-effect morphological regimes occurred over the western Great Lakes on 25 January 2000 (Fig. 1). Figure 1 shows a *shoreline band* over Lake Michigan. This type of lake-effect event typically develops due to a thermally driven land-breeze circulation and/or prevailing winds nearly parallel to the major axis of the lake; often results in localized, heavy snowfall amounts; and produces the largest vertical motions associated with lake-effect

events (e.g., Passarelli and Braham 1981). A *widespread coverage* event; consisting of cellular convection and wind-parallel bands, occurred over and downwind of Lake Superior. This type of event is typically associated with unidirectional winds across the lake and light to moderate widespread snowfall over and downwind of the lake (e.g., Kelly 1986). Over Lake Huron, a cyclonic *mesoscale vortex* developed. Lake-effect vortices are often associated with light snowfall, weak land-breeze winds along all shorelines, and may have a cloud-free region near the center of the circulation (e.g., Laird 1999).

The determination of the environmental conditions that favor an individual meso-β-scale lake-effect morphological regime over another is the primary objective of the current investigation. Hjelmfelt (1990) provided the only previous comprehensive investigation of the influence of environmental parameters on determining different lake-effect morphological regimes; however, Hjelmfelt (1990) placed particular emphasis on the conditions favorable for land-breeze development along the eastern shore of Lake Michigan. As a consequence of previous research only focusing on specific lake-effect events (i.e., case studies) or particular morphological regimes, a collective comprehensive understanding has not been developed of the conditions that support each lake-effect morphological regime and the parametric boundaries between regimes. Our investigation used a large array of idealized three-dimensional mesoscale model simulations of stratified airflow over a relatively warm circular lake to supply practical information for the prediction of 1) the morphological regime of a mesoscale lake-effect circulation and 2) periods of regime transition.

Information concerning the mesoscale model used for this study is included in section 2. Dimensional analysis of the lake-effect system is presented in section 3. Characteristics of each lake-effect regime are described in section 4. Parameters previously used for classification of the structure of mesoscale circulations are discussed in section 5. The determination of a predictive quantity that can be used to classify lake-effect morphological regime is presented in sections 6 and 7. Discussion and conclusions are provided in section 8.

2. Mesoscale model

The Colorado State University Mesoscale Model (CSUMM) used for this investigation is a three-dimensional, hydrostatic, incompressible, primitive-equation model originally developed by Pielke (1974) to study the Florida sea-breeze circulation. The CSUMM has been modified and enhanced over the past 25 years and used extensively to simulate thermally and topographically forced mesoscale flows. For example, Hjelmfelt and Braham (1983), Pease et al. (1988), and Hjelmfelt (1990) have used the CSUMM to successfully simulate lake-effect snowstorms over Lake Michigan. The basic model formulation is provided by Mahrer and Pielke (1977) and the numerical advection scheme is described by Mahrer and Pielke (1978). Additional details of the CSUMM are provided in Pielke (1984). We give only a brief description of the model features. A complete description of the model version used for this study is contained in Laird (2001).

a. Model description

The CSUMM uses a terrain-following vertical coordinate $z^* = s(z - z_t)/(s - z_t)$, where z is height above sea level, z_t is terrain height, and s is the fixed height of the model top. For our study, the CSUMM grid was equivalent to a Cartesian grid since flat, sea level topography was utilized for the simulations. Near the lower boundary, surface layer similarity theory is used to parameterize fluxes based on the heat, moisture, and momentum flux-profile relationships of Businger et al. (1971). The vertical turbulent exchange coefficients are derived from the predicted local turbulent kinetic energy and boundary layer depth (Ulrickson and Mass 1990).

For this study, atmospheric water vapor was considered a passive scalar quantity that could be advected by the wind, diffused by turbulence, and exchanged (i.e., depleted or enhanced) at the surface. In an effort to reduce large computational time and model output storage capacity for the 35 model simulations performed, latent heating and precipitation processes were not included. Previous lake-effect investigations (i.e., Hjelmfelt and Braham 1983; Hjelmfelt 1990; Cooper et al. 2000) have shown that lake-induced circulations maintain their structure in the absence of moist microphysical processes and associated latent heating, even though their strength may be reduced by nearly 50%. While these studies provide evidence of the impact of latent heating on mesoscale structure, the full effect may not be recognized since the cases examined may not have been near lake-effect morphological regime boundaries. In addition, solar radiation calculations were not included in the simulations. The mesoscale forcing by differential solar heating at the lake–land boundary has been found to be significantly less intense than the differential diabatic forcing due to the flow of arctic air over the warm lake waters (e.g., Chang and Braham 1991).

b. Initialization and boundary conditions

The model requires input of gridded terrain information (topographic elevations, water/land coverage) and vertical profiles of temperature, specific humidity, and wind. The initial wind profile is used to establish both the initial uniform wind field throughout the domain and the geostrophic winds, which in combination with the Coriolis parameter supply a constant, uniform, large-scale pressure gradient term in the horizontal momentum equations.

Zero-gradient lateral boundary conditions were assumed for all prognostic variables. In addition, the lateral boundaries were far removed from the region of interest to avoid contamination of the model solution by boundary effects. At the lower boundary, a no-slip condition was specified for the horizontal velocities ($u = v = 0$) and the vertical velocity was $w = 0$. The model initialization included a modified Ekman-balanced boundary layer in order to incorporate surface friction into the initial wind field. The upper boundary was an isentropic surface with constant horizontal velocity. The highest three levels composed a viscous absorbing layer. In this layer, Rayleigh friction was applied to the velocity perturbations and Newtonian cooling was applied to the potential temperature perturbations to damp upward-propagating disturbances and prevent downward reflection into the domain (Klemp and Durran 1983).

c. Model domain and idealized experiments

The model simulations were performed on a 76 × 76 × 20 grid. The horizontal grid spacing was 10 km, except for the first three grid intervals inward from each lateral boundary, which were 80, 40, and 20 km, respectively. Flat topography was used, and the heights of the vertical levels were $z = 0.01$, 0.03, 0.06, 0.1, 0.25, 0.5, 0.75, and 1.0 km with the remaining levels separated by 0.5 km from 1.0 to 4.0 km and by 1.0 km from 4.0 to 10.0 km.

A single axisymmetric lake having a diameter of 100, 200, or 300 km was located near the center of the domain. The surface areas of these idealized circular lakes were 7850, 31 400, and 70 700 km^2, respectively. These values are comparable to those of several individual Great Lakes, where Lakes Superior, Huron, Michigan, Erie, Ontario, and St. Clair have surface areas of 82 200, 59 600, 57 800, 25 700, 19 000, and 1300 km^2, respectively. Surface roughness length was assumed to be 5 cm over land and computed as a function of wind speed over the lake surface. A constant, uniform lake surface water temperature of 273 K was prescribed. Initial 10-m air temperatures ranged from 265.5 to 250.5 K. Both observational (e.g., Passarelli and Braham 1981; Kelly 1984; Laird 1999) and modeling (e.g., Hjelmfelt 1990) lake-effect investigations have demonstrated that values of ΔT greater than about 5°–10°C are generally required for meso-β-scale lake-effect circulations to develop when synoptic-scale flow exists. Therefore, the results discussed in the current study were obtained for simulated conditions where ΔT was greater than 5°C.

The initial sounding contained 50% and 25% relative humidity layers from 0.0 to 0.1 km and 0.1 to 10.0 km, respectively. A constant initial stability existed from the surface to 1.5 km ($d\theta/dz = 1.0$, 3.0, or 6.0 K km^{-1}). From 1.5 to 3.5 km a stable layer was prescribed as a transition from the constant lapse rate below to $d\theta/dz = 8.0$ K km^{-1} above 3.5 km. Similar profiles containing a well-mixed boundary layer capped by an inversion or stable layer have often been observed upwind of lakes during lake-effect events (e.g., Hjelmfelt and Braham 1983; Laird 1999) and used in prior idealized lake-effect modeling investigations (e.g., Hjelmfelt 1990; Sousounis 1993; Rose 2000).

Wind profiles were prescribed using a nearly uniform speed and direction (westerly winds) throughout the entire profile. The initial wind field was slightly modified with an assumed Ekman-balanced boundary layer. Initial wind speeds ranging from 0.0 to 18.2 m s^{-1} were used under a variety of environmental conditions.

Thirty-five model simulations were performed using varied wind speed, lake − air temperature difference, atmospheric stability, and lake diameter. Each was performed using a constant value of Coriolis parameter at 44° latitude. The parameters used for each model simulation are shown in the appendix A. The specifications of the various idealized atmospheric environments were based on typical conditions observed during Arctic cold-air outbreaks and previously observed lake-effect conditions in the Great Lakes region (e.g., Braham and Kelly 1982).

Past studies of thermally driven circulations (e.g., lake-effect, sea breeze, etc.) have used several variables to examine the intensity of the resulting mesoscale response. Similarly, the intensity of the lake-effect circulations simulated in this investigation was primarily indicated by maximum vertical velocity. Several additional measures of intensity were also examined, such as sea level pressure perturbation and maximum convergence, both of which were correlated with maximum vertical velocity and yielded similar results.

A 36-h simulation was performed for each experiment using a time step of 40 s. This allowed the initially uniform conditions to respond to the positive (i.e., surface to atmosphere) heat fluxes associated with the relatively warm axisymmetric lake and inhomogeneous surface friction. The presented results use model output at the 24-h simulated time. By 24 h, the mesoscale circulation had generally reached maximum intensity and a quasi-steady circulation was sustained in each simulation. For example, Fig. 2 shows the time series of the three-dimensional domain maximum vertical velocity for each of the 35 simulations.

3. Dimensional analysis of the lake-effect system

The dimensional analysis technique was applied to examine the combined effects of varied environmental and surface conditions used in the 35 simulations. Dimensional analysis is a technique that has been used for many years to obtain preliminary solutions to physical problems and is outlined in numerous fluid mechanics texts (e.g., Kundu 1990; Stull 1988). Assuming that the specified system can be described by a set of variables, dimensional analysis can be used to determine a general

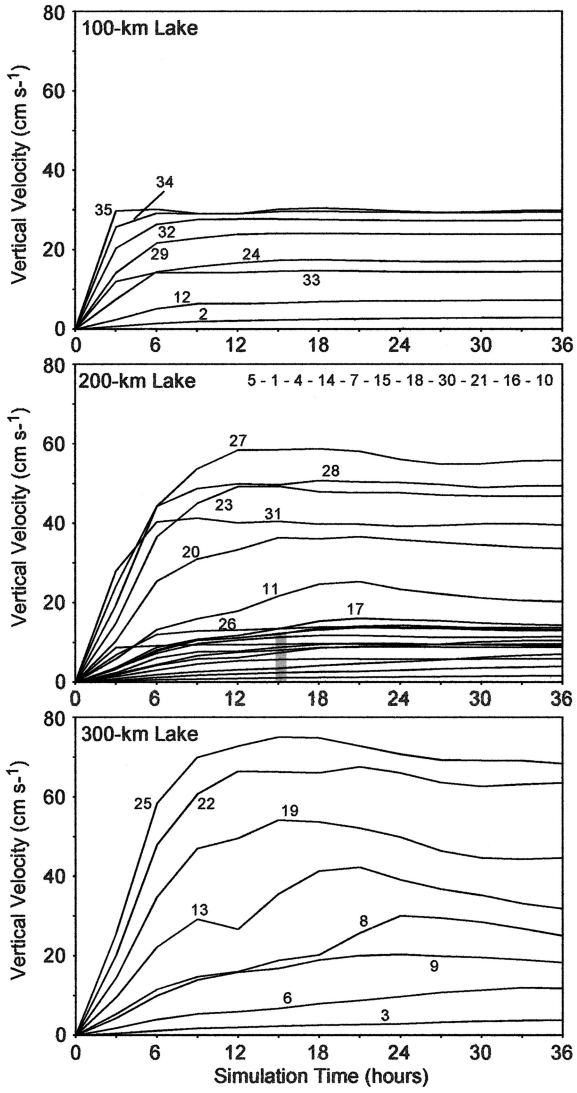

FIG. 2. Time series of three-dimensional domain maximum vertical velocity for all 35 simulations. The numbers denote the simulation number shown in the appendix. The thick gray line in the 200-km lake panel is used to identify the simulation number (shown at the top of panel) from bottom of line to top.

form of the solution from dimensional constraints. Dimensional analysis is most useful for problems where the derivation of an analytical solution is difficult but the variables that compose the system being examined are generally understood. This is the case for winter lake-effect systems where the mesoscale circulations are complex and exhibit several types of structures (e.g., vortices, shoreline bands); however, the basic environmental variables that influence the system are reasonably well known (e.g., lake − air temperature difference, wind speed). Although dimensional analysis can provide insight into a complex multivariate problem, it does not provide the ability to obtain a complete solution or adequately describe the physical processes that contribute to the system (Vignaux 1986).

Previous lake-effect investigations (e.g., Hjelmfelt 1990; Sousounis 1993; Kristovich and Laird 1998) and studies of stratified flow over an isolated surface heat source (e.g., Lin 1986; Hsu 1987b; Lin 1989; Xie and Lin 1996) have demonstrated the significance of individual variables to the development of a mesoscale response circulation. Consider that the following function of fundamental variables describes a lake-effect system:

$$f(U, L, H, \rho, T, \Delta T, p, N, f) = 0, \qquad (3.1)$$

where U is the ambient wind speed not influenced by frictional drag, L is maximum fetch distance (i.e., lake diameter), H is the boundary layer depth upwind of the lake, ρ is air density, T is 10-m air temperature upwind of the lake, ΔT is the temperature difference between the lake surface and T, p is pressure, N is Brunt–Väisälä frequency, and f is the Coriolis parameter. Variables were selected that are easily obtained from routine measurements and are standard model output variables. This allows the dimensionless parameters (i.e., π groups) developed to be calculated in a straightforward manner. It may also allow parameters from previously completed mesoscale lake-effect observational studies to be compared to the findings from this numerical modeling investigation. From the nine fundamental variables, the following dimensionless π groups were determined using the Buckingham Pi theorem (Buckingham 1914):

$$f\left(\frac{H}{L}, \frac{\Delta T}{T}, \frac{p}{\rho U^2}, \frac{U}{NL}, \frac{U}{fL}\right) = 0. \qquad (3.2)$$

Since the Euler number, $p/\rho U^2$, is typically associated with externally forced motions, it was considered independent of thermally induced lake-effect circulations. Manipulation of the π groups is permitted provided the number of π groups involved is not changed. Dimensionless π groups, which include the Rossby number [Ro = $U/(fL)$] and the Froude number {Fr = $[U/(NL)](L/H)$ = $U/(NH)$}, were used to examine the mesoscale structure of lake-effect circulations.

4. Lake-effect structures

The criteria used to differentiate the meso-β-scale lake-effect structures within the model output were primarily based on the examination of near-surface wind fields for characteristic features associated with each lake-effect morphological regime. A mesoscale vortex was identified when a closed cyclonic circulation was exhibited in the low-level wind field. The diameter of the simulated cyclonic vortex varied from lake scale (e.g., 200 km) to approximately 40 km. In the presence of background flow, the vortex circulation was located either over the downwind half of the lake or in the vicinity of the downwind shoreline. The presence of a land-breeze wind component confined near the downwind shore and a line of convergence over the lake in the model-simulated wind field was used to identify

shoreline band events. This definition is consistent with both observations of intense lake-effect band events (e.g., Passarelli and Braham 1981; Braham 1983; Schoenberger 1986) and the definition used by Hjelmfelt (1990) when examining simulated shoreline bands. A widespread coverage event was identified when the downwind-shore land breeze and an overlake convergence band or vortex did not exist.

Although pronounced features associated with each type of morphological regime were used, the determination of the appropriate lake-effect morphological regime for each simulation was subjective in some cases. The output from most of the model simulations contained easily identifiable features associated with a single lake-effect morphological regime; however, a limited number of simulations produced circulations with features of two regimes. The environmental conditions that led to the development of a mesoscale circulation with features from two morphologies were found to be associated with transition zones between the major regimes.

Figure 3 presents the simulated 10-m wind, surface pressure, and 1500-m vertical motion fields for a mesoscale vortex, shoreline band, and widespread coverage event. Figures 3a and 3b show a lake-scale cyclonic vortex centered over the downwind half of the lake, a surface pressure perturbation of approximately -1.5 hPa, and weak vertical motions associated with the vortex circulation of 2.5–5.0 cm s^{-1}. These characteristics are consistent with observations discussed by Forbes and Merritt (1984), Pease et al. (1988), and Laird (1999). For example, Forbes and Merritt (1984) found that small reductions in sea level pressure ($\sim$1 hPa) are generally associated with a lake-effect vortex.

A simulated shoreline band over the downwind lakeshore is presented in Figs. 3c and 3d. The 10-m simulated winds in the northeastern region downwind of the lake contain a lakeward component that is indicative of a land breeze. The other simulated fields show a surface pressure perturbation of nearly -2.5 hPa located at the southern end of the shoreline band, a reduction in surface pressure extending several hundred kilometers downwind of the lake, and vertical motions of 10–45 cm s^{-1} along the band. The reduced surface pressure and stronger vertical motions associated with the simulated shoreline band are reasonably consistent with observations presented by Braham (1983) of 1.0–4.0-hPa pressure decreases and 0.5–1.0 m s^{-1} vertical motions associated with a narrow, intense shoreline snowband positioned along the eastern shore of Lake Michigan during 8–11 December 1977.

Figures 3e and 3f show a simulated widespread coverage event. It is important to note that although there are regions of low wind speeds and weak convergence downwind of the lake, a land-breeze component is not present in the 10-m wind field. In comparison with the shoreline band event (Figs. 3c and 3d), the mesoscale low pressure center located near the downwind shore is slightly deeper (i.e., pressure perturbation of -3.0 hPa) and the magnitude of the maximum vertical motions is lower [i.e., w_{max} (1500 m) = 30 cm s^{-1}]. These vertical motions are similar to values of 20–50 cm s^{-1} estimated by Kristovich (1993) from radar measurements of wind-parallel lake-effect bands (i.e., widespread coverage). Although wind-parallel bands and cellular convection are typically observed during widespread coverage events, our use of a 10-km horizontal grid interval does not allow simulation of meso-γ-scale convective features.

Figure 4 quantifies the spatial area influenced by easterly land-breeze flow and the maximum easterly wind speed downwind of the lake for each simulation (see the appendix for conditions associated with each model simulation). Simulations with relatively extensive land-breeze flow are associated with lake-effect mesoscale vortex events (i.e., simulations 1–7). Simulations resulting in localized land-breeze flow in the vicinity of the downwind shoreline corresponded to shoreline band events (i.e., simulations 8–29) and easterly flow was absent during widespread coverage events (i.e., simulations 30–35).

The area influenced by land-breeze flow, the maximum easterly wind speed, and the strength of a land-breeze convergence zone also provide some information about the complex interrelationship that variations in environmental variables have on the intensity of lake-effect events (e.g., Hjelmfelt 1990). For example, a larger area of land-breeze flow, greater easterly wind maximum, and greater vertical velocity maximum are associated with the shoreline band that develops in simulation 10 (U = 4.8 m s^{-1}, ΔT = 16°C, L = 200 km) when compared to the band in simulation 12 (U = 2.5 m s^{-1}, ΔT = 22.5°C, L = 100 km). Although ΔT is larger for simulation 12, Fig. 4 shows simulations 10 and 12 develop land breezes with areas of 610 and 200 km^2, respectively, and maximum easterly wind speeds of 2.01 and 0.70 m s^{-1}, respectively. In addition, the bands that develop in simulations 10 and 12 have maximum vertical velocities of 14.30 and 7.12 cm s^{-1}. Further studies are necessary to address the influence of these complex interrelationships on the intensity of each morphological regime.

5. Previous classification of lake-effect mesoscale structures

a. Wind speed versus ΔT parameter space

Past investigations of lake-effect storms (e.g., Hjelmfelt 1990), boundary layer convection (e.g., Woodcock 1940; Priestley 1957; Grossman 1982), and thermally driven mesoscale circulations (e.g., Biggs and Graves 1962; Walsh 1974) have typically used the two-dimensional parameter space of wind speed versus water−air temperature difference to identify suitable conditions for a particular type of mesoscale structure. Based on the

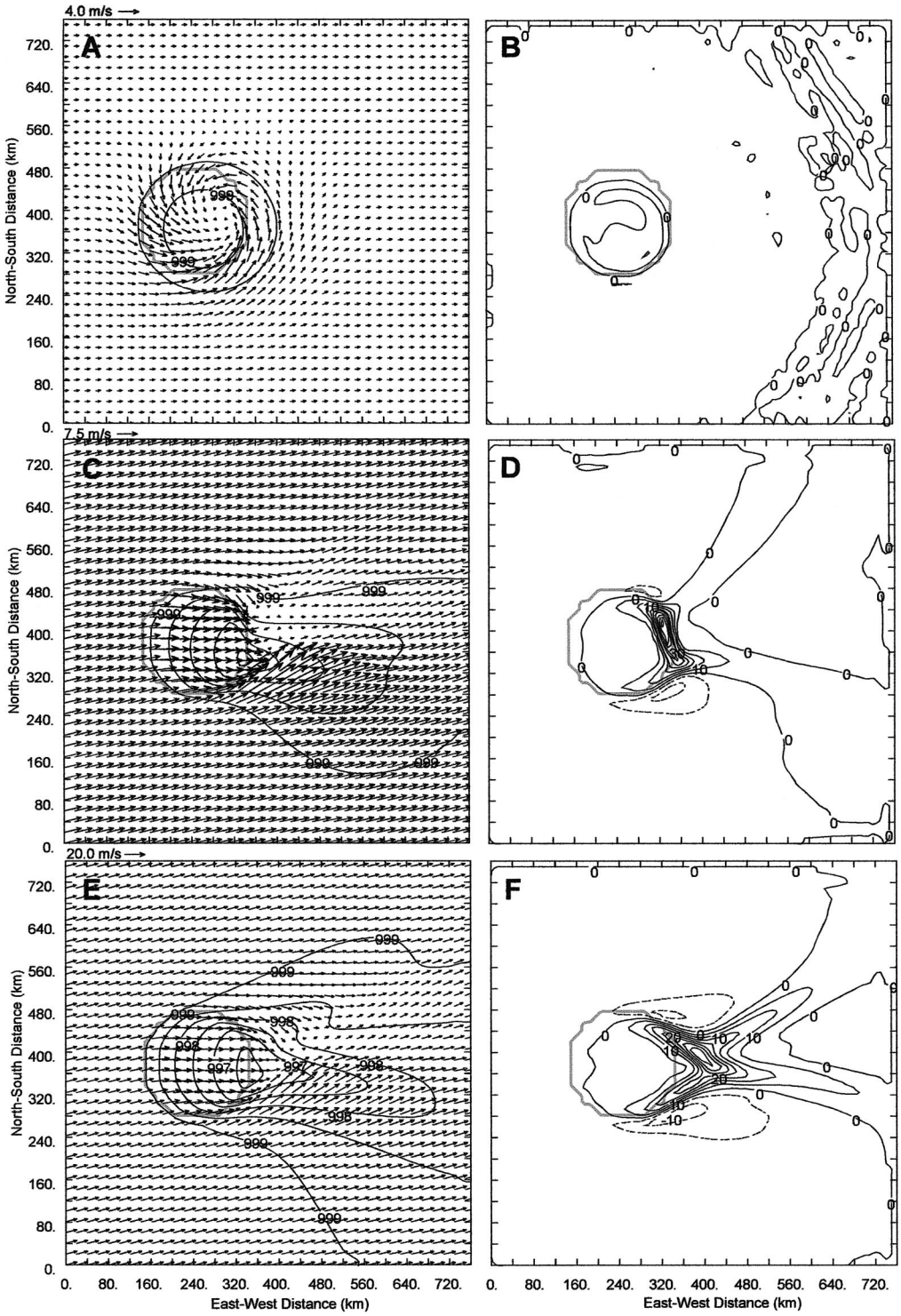

FIG. 3. Examples of the 10-m wind, surface pressure (left column), and 1500-m vertical motion (right column) fields for the three primary lake-effect morphological regimes. (a), (b) Vortex with initial condition of $U = 1.0$ m s^{-1}. Arrows are scaled to 4.0 m s^{-1}. (c), (d) Shoreline band with initial condition of $U = 10.0$ m s^{-1}. Arrows scaled to 7.5 m s^{-1}. (e), (f) Widespread coverage with initial condition of $U = 18.2$ m s^{-1}. Arrows scaled to 20.0 m s^{-1}. All simulations had $L = 200$ km, $\Delta T = 22.5$°C, and $N = 0.006$ s^{-1}. Solid (dashed) contours represent positive (negative) values.

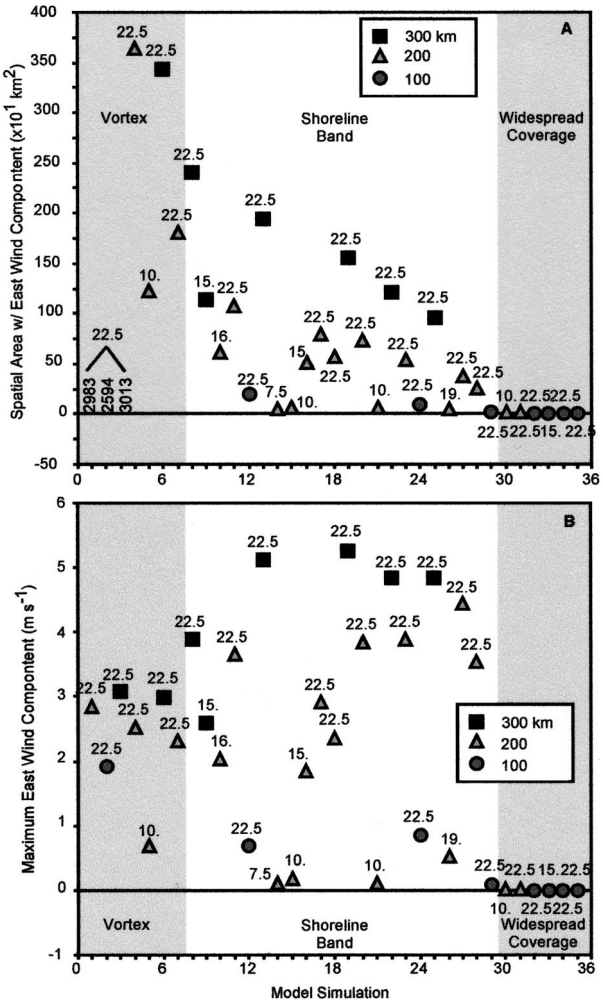

FIG. 4. Plot of (a) spatial area of easterly wind component and (b) maximum east wind component at 10 m for each model simulation. Symbols represent lake diameter and labels are ΔT values of simulations. Areas ($\times 10^1$ km^2) for simulation 1, 2, and 3 are given. The morphological regime is also shown.

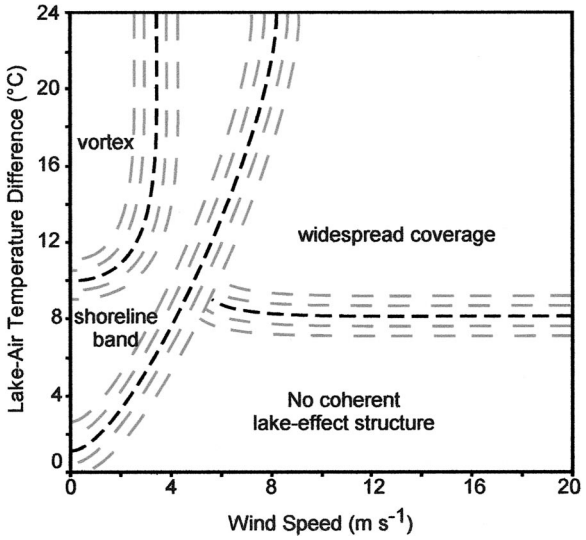

FIG. 5. Diagram showing general conditions favorable for different lake-effect morphological regimes using wind speed vs lake–air temperature difference parameter space. The diagram is a composite based on the existing lake-effect literature. The dashed lines represent nondistinct boundaries between regimes.

existing lake-effect scientific literature, Fig. 5 presents a composite diagram of general conditions favorable for different lake-effect structures. Widespread coverage events most often occur with strong wind speeds and $\Delta T > 7$°C. Shoreline bands generally occur with moderate to weak wind speeds and ΔT ranging from small to large positive values (e.g., 5°–24°C). Last, lake-effect mesoscale vortex events have been most frequently observed with weak wind speeds and $\Delta T > 10$°C.

An important disadvantage of using the U versus ΔT diagram for the prediction of lake-effect morphological regime is different lake-effect mesoscale structures (e.g., vortex, shoreline band) can occur under identical U and ΔT conditions since additional factors, such as lake size and shape, can aid in determining the structure. These factors are not accounted for in the U versus ΔT diagram. Therefore, a single parameter that can better classify or predict the mesoscale structure is desirable and could be used in combination with a parameter that describes the circulation intensity to form a two-dimensional parameter space providing a clear distinction between structure and intensity information. In this study, we examine several parameters that may be used to classify lake-effect mesoscale structure.

b. Parameters used for classification of mesoscale structures

Investigations of uniform stratified airflow over a two-dimensional near-surface mesoscale heat source using linear theory (e.g., Lin and Smith 1986; Lin 1986; Hsu 1987b) have shown that for nonrotating airflow the phase relationship between the heat source and the induced vertical motion depends on Fr. When Fr $\ll 1$, the region of ascent occurs primarily over the heat source. As Fr increases, the center of the ascending region relocates downstream, while a region of descent shifts toward the heat source from upstream. When Fr > 1, a negative phase relationship is reached and the center of the descending region is located over the heat source.

More recently, Sousounis and Shirer (1992) and Sousounis (1993) used numerical model investigations to examine the atmospheric response to a prescribed lake-effect environment. Using a two-dimensional, linear, analytic model to examine lake-aggregate disturbances (i.e., horizontal heat source diameter of 500 km), Sousounis and Shirer (1992) found a nonoscillatory (oscillatory) response existed for Fr < 1 (Fr > 1). For Fr $= 1$, a response characterized by extremely large amplitudes and relatively small spatial extent was found. Using a two-dimensional nonlinear mesoscale model to

examine wind speed effects on lake-effect storms, Sousounis (1993) found that the wind speed for maximum snowfall near the downwind lakeshore of a 200-km lake yielded an Fr very close to unity and suggested that Fr may be a useful parameter for the forecasting of lake-effect storms.

In another relevant study, Xie and Lin (1996) used a numerical model to investigate the response of stratified airflow to a prescribed near-surface mesoscale heat source. Using three simulations with axisymmetric heat sources of 30- or 70-km diameters, Xie and Lin (1996) suggested that the intensity of the mesoscale response decreases as Ro increases and that Fr largely determines the horizontal structure of the response. Xie and Lin (1996) note several limitations of their study, such as the diabatic heating field was prescribed and did not allow for feedback from the kinematic field. Several aspects extremely relevant to lake-effect and other thermally induced mesoscale systems could not be examined using the sets of model simulations performed in the studies of Sousounis and Shirer (1992), Sousounis (1993), and Xie and Lin (1996). These include 1) variations in the magnitude of surface heating, 2) variations in the atmospheric stability, and 3) spatial variations of surface friction within an x–y plane.

The dependence of the structure of mesoscale circulations on Fr may not be surprising since the hydrostatic atmospheric response to the heat source and localized atmospheric region of heating interacts with the gradient flow to produce circulations similar to those that develop from flow over an isolated mountain (e.g., Smith 1988; Bauer et al. 2000) or island (e.g., Smith and Grubisic 1993). Analogous to the importance of the slope and height of a topographic obstacle, the magnitude (i.e., ΔT) and atmospheric depth of heating associated with a surface heat source can contribute to determining the structure of the atmospheric response.

Several previous research investigations of lake-effect circulations and stratified flow over an isolated surface heat source have suggested Fr may be useful for identifying the mesoscale structure. The dimensional analysis presented in section 3 also suggested several parameters may prove useful in predicting the lake-effect morphological regime. Analyses showed that H/L and $\Delta T/T$ were unsuccessful in classifying lake-effect morphological regimes. Therefore, the utility of only Fr and Ro as predictors of lake-effect morphological regime are examined in sections 6 and 7.

6. Structure sensitivity to Froude number

The Fr was both determined through dimensional analysis as a dimensionless parameter and suggested by previous investigations (e.g., Sousounis 1993; Xie and Lin 1996) as a potential parameter useful for classifying the structure of lake-effect circulations. The current set of simulations examined variations in Fr using an array of environmental conditions (i.e., stability, T, U, and lake diameter) to determine the effectiveness of Fr in differentiating mesoscale lake-effect structures. For the current investigation, Fr was derived using model initial conditions and defined as $\mathrm{Fr} = U/(NH)$, where U is the ambient wind speed above the influence of surface friction, N is the lower-tropospheric Brunt–Väisälä frequency, and H is the boundary layer depth upwind of the lake.

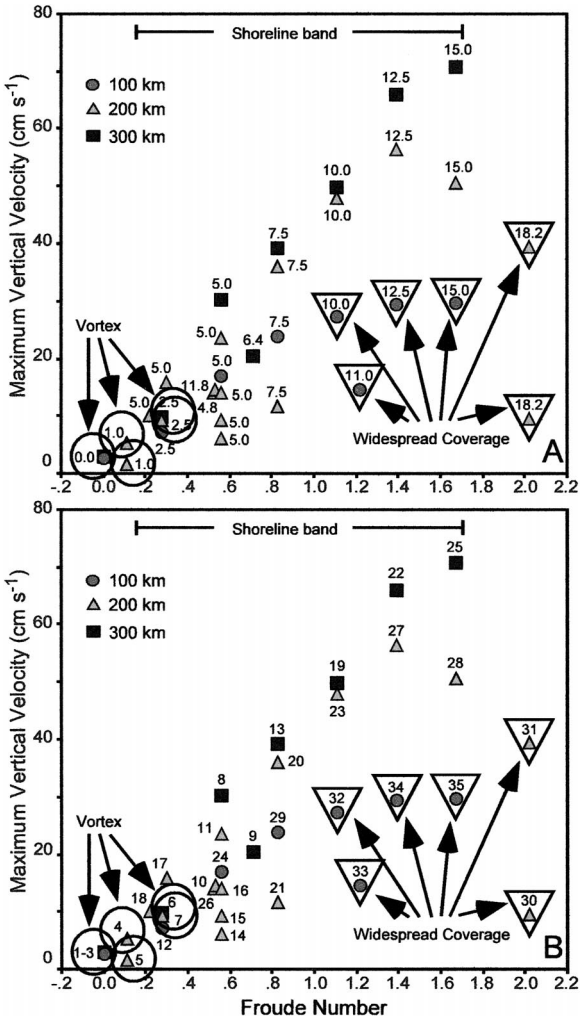

FIG. 6. Froude number vs maximum vertical velocity. Labels identify results by (a) ambient wind speed (m s^{-1}) and (b) simulation number from the appendix. Lakes of 100- (circles), 200- (triangles), and 300-km (rectangles) diameter are shown. Mesoscale vortex and widespread events are noted with large circles and triangles, respectively.

Figure 6 shows the relationships of Fr to maximum vertical motion and the mesoscale structure of the lake-effect circulation from each of the 35 simulations. The Fr is noticeably associated with the mesoscale structure of the response circulations. Mesoscale vortex and widespread coverage events are confined to lower (<0.4) and higher (>1.0) Froude numbers, respectively. However, shoreline band events span the entire range of

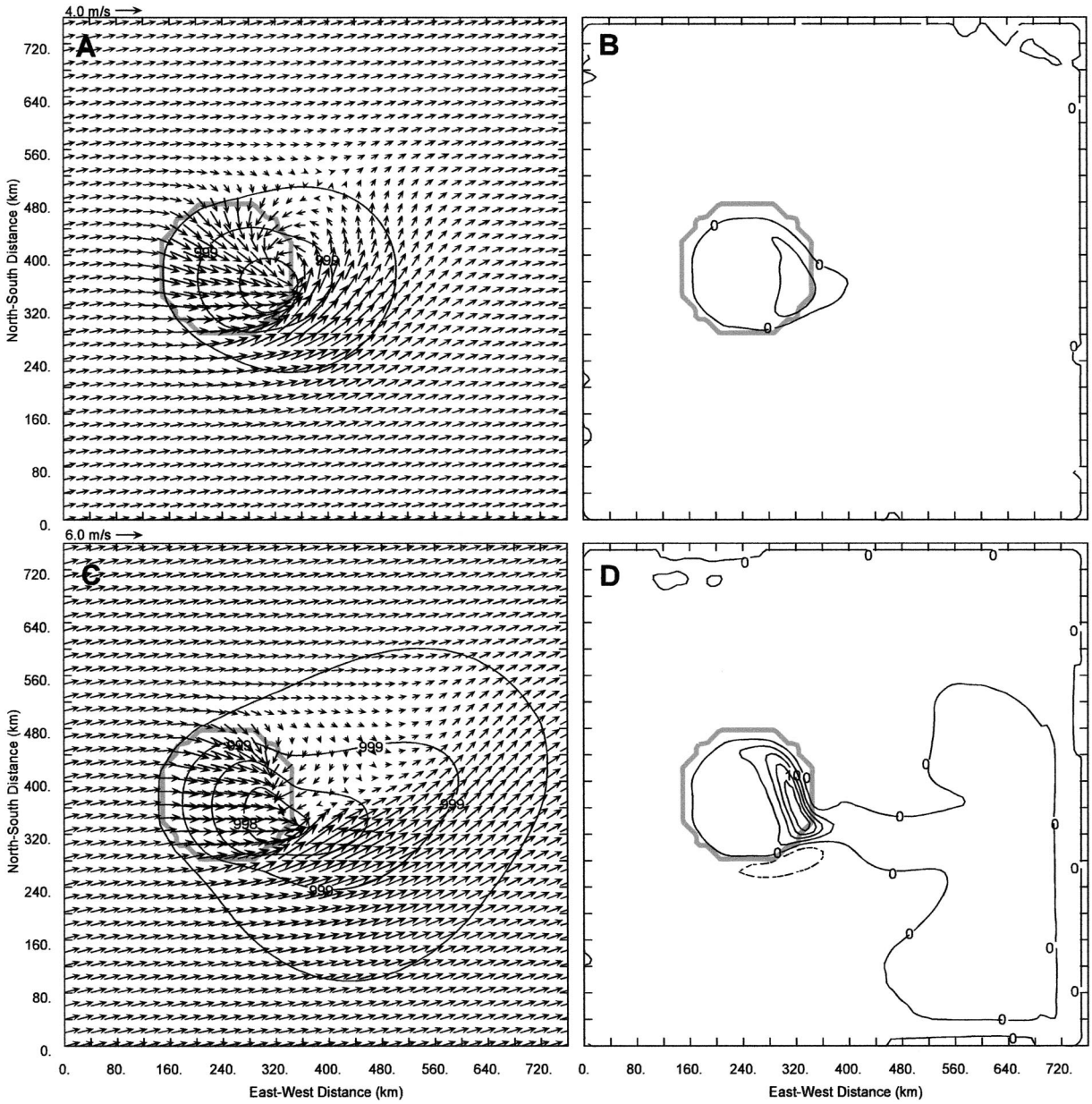

FIG. 7. The 10-m wind, surface pressure, and 1500-m vertical motion fields for (a), (b) a mesoscale vortex with Fr = 0.28, Ro = 0.12 (U/L = 0.012 m s^{-1} km^{-1}), U = 2.5 m s^{-1}, and N = 0.006 s^{-1} and (c), (d) shoreline band with Fr = 0.30, Ro = 0.25 (U/L = 0.025 m s^{-1} km^{-1}), U = 5.0 m s^{-1}, and N = 0.011 s^{-1}. The contour intervals of pressure and vertical velocity are 0.5 hPa and 5.0 cm s^{-1}, respectively. The simulation used L = 200 km and ΔT = 22.5°C.

Froude numbers in addition to being uniquely predicted at intermediate values ($0.4 < \text{Fr} < 1.0$).

Two examples are shown where the environmental conditions resulted in nearly equivalent Froude numbers, but the structure of the resulting lake-effect circulation differed substantially. The first example presents circulations from the mesoscale vortex and shoreline band regimes that occur with similar Froude numbers. Figure 7 compares the 10-m wind, surface pressure, and 1500-m vertical motion fields from the two simulations. Figures 7a and 7b show results from the simulation having initial conditions of Fr = 0.28, U = 2.5 m s^{-1}, and N = 0.006 s^{-1}. A meso-β-scale vortex with a diameter of approximately 150 km is located over the downwind lakeshore. Weak vertical motions (<10 cm s^{-1}) are associated with the vortex circulation. Figures 7c and 7d show results from the simulation with initial conditions of Fr = 0.30, U = 5.0 m s^{-1}, and N = 0.011 s^{-1}. A shoreline band developed over the lake near the downwind shore. Convergence of the 10-m winds is clearly evident in the vicinity of the band and enhanced vertical motions of nearly 25

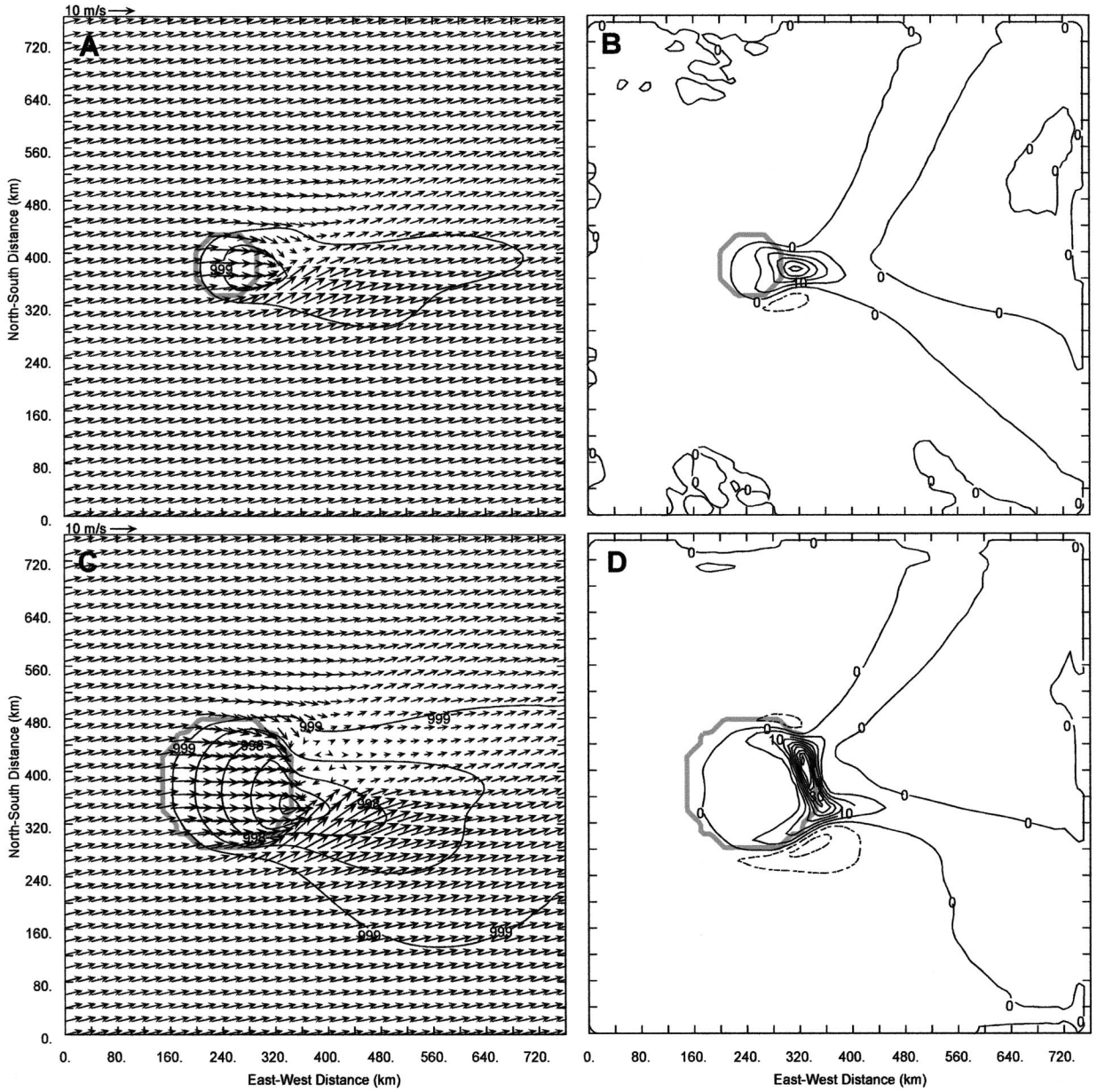

FIG. 8. The 10-m wind, surface pressure, and 1500-m vertical motion fields for (a), (b) a widespread coverage event with Fr = 1.11, Ro = 0.99 (U/L = 0.099 m s^{-1} km^{-1}), and L = 100 km and (c), (d) shoreline band with Fr = 1.11, Ro = 0.49 (0.049 m s^{-1} km^{-1}), and L = 200 km. Each simulation used U = 10.0 m s^{-1}, N = 0.006 s^{-1}, and ΔT = 22.5°C. Contour intervals of pressure and vertical velocity are 0.5 hPa and 5.0 cm s^{-1}, respectively.

cm s^{-1} are collocated with the position of the shoreline band. This comparison shows that an Fr of approximately 0.3 would indicate the possible development of either a mesoscale vortex or a shoreline band.

The second example presents circulations from the widespread coverage and shoreline band regimes that occur with similar Froude numbers. Figure 8 compares the 10-m wind, surface pressure, and 1500-m vertical motion fields from the two simulations. Figures 8a and 8b show results from the simulation having initial conditions of Fr = 1.11, U = 10.0 m s^{-1}, and L = 100 km. A widespread coverage event is located over and downwind of the lake. Maximum vertical motions of nearly 25 cm s^{-1} are associated with the widespread lake-effect circulation. Figures 8c and 8d show results from the simulation with initial conditions of Fr = 1.11, U = 10.0 m s^{-1}, and L = 200 km. An intense shoreline band developed over the downwind shore. Enhanced vertical motions of approximately 50 cm s^{-1} are associated with the shoreline band. This comparison shows Fr = 1.0 is associated with the possible development of either a shoreline band or widespread coverage event.

Although Fr is noticeably associated with the structure of the response circulations, our results suggest that Fr alone may be of limited use as an aid in forecasting the mesoscale lake-effect structure.

7. Structure sensitivity to Rossby number and *U*/*L*

The Ro was determined through dimensional analysis as another dimensionless parameter that may be used to describe the lake-effect system. In addition, Ro has been cited by previous authors as useful for describing characteristics of mesoscale circulations. For this study, the Ro was based on environmental conditions used for model initialization and defined as $\mathrm{Ro} = U/(fL)$, where U is the ambient wind speed, f is the Coriolis parameter, and L is the maximum fetch distance (i.e., lake diameter). Changes in latitude (i.e., Coriolis forcing) were examined with additional sensitivity simulations (not included in the set of 35) and, similar to findings of Hjelmfelt (1990), were found to have a secondary influence on the structure of lake-effect circulations. Therefore, the primary quantity of interest in this section for the classification of lake-effect structure is the ratio of wind speed to maximum fetch distance (U/L).

Figure 9 shows the relationships of U/L to the maximum vertical motion and mesoscale structure of the lake-effect circulation from each of the 35 simulations. Details of each of the simulations are presented in the appendix. The quantity U/L was successful in differentiating the three basic lake-effect morphological regimes. Lake-effect environmental conditions producing low values of U/L (i.e., approximately < 0.02 m s^{-1} km^{-1}) resulted in a mesoscale vortex circulation. Conditions leading to U/L values between about 0.02 and 0.09 m s^{-1} km^{-1} resulted in the development of a shoreline band, and U/L values greater than approximately 0.09 m s^{-1} km^{-1} produced a widespread coverage event over and downwind of the lake. It is important to emphasize that a structural transition from one morphological regime to another is continuous and the shaded bands on Fig. 9 do not represent sharp, distinct boundaries. Given a finite number of simulations, it is difficult to accurately determine the width of these transition zones. Additionally, within these transitional zones the structure of a lake-effect circulation may contain features characteristic of more than one morphological regime, similar to observed lake-effect events with complex, combined mesoscale structures (e.g., Pitts et al. 1977; Laird 1999).

The previously cited examples in Figs. 7 and 8 provide comparisons of the use of U/L and Fr to predict the lake-effect morphological regime. Although the lake-effect circulations shown in Fig. 7 have nearly equivalent Froude numbers ($\sim$0.3), the different U/L values of the mesoscale vortex ($\mathrm{Ro} = 0.012$ m s^{-1} km^{-1}) and shoreline band ($U/L = 0.025$ m s^{-1} km^{-1}) clearly distinguish the lake-effect morphological regimes. Similarly, the U/L values associated with the widespread coverage event ($U/L = 0.099$ m s^{-1} km^{-1}) and shoreline band ($U/L = 0.049$ m s^{-1} km^{-1}) shown in Fig. 8 successfully differentiate the two lake-effect regimes.

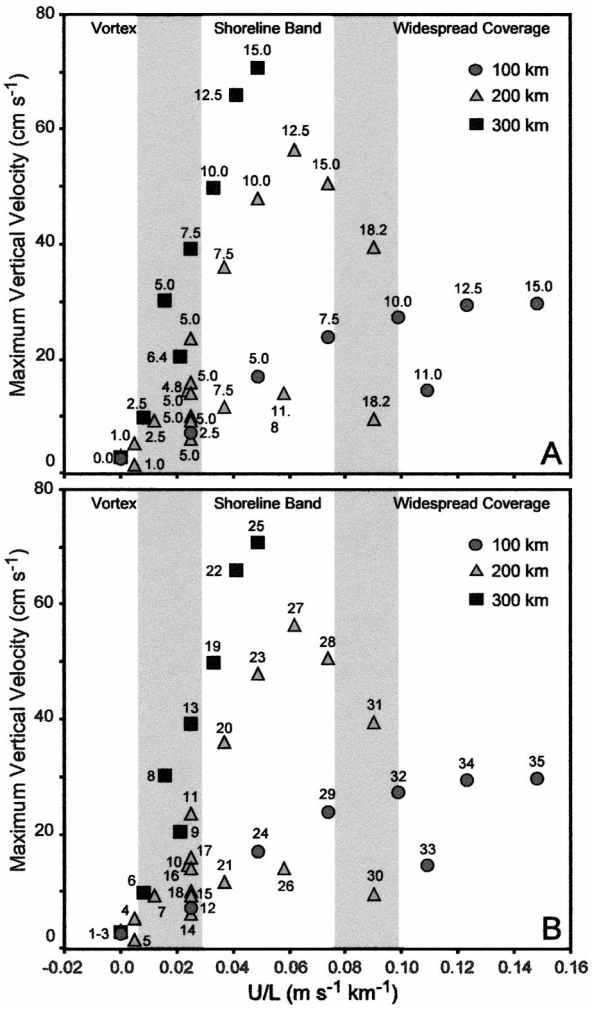

FIG. 9. The U/L vs maximum vertical velocity. Labels identify results by (a) ambient wind speed (m s^{-1}) and (b) experiment number from the appendix. Axisymmetric lakes of 100 (circles), 200 (triangles), and 300 km (rectangles) are shown.

Figure 10 presents an additional example comparing two simulations with equivalent values of U/L and different values of Fr. The resulting mesoscale circulations have very similar structure, as seen in the 1500-m vertical motion and 10-m wind fields. Shoreline convergence bands develop and contain vertical motions of similar magnitude near the downwind shoreline in each simulation. Additional results from simulations 11–18, where U, ΔT, N, L, and Fr values vary, show that equivalent values of U/L predict the same morphological regime (shoreline band) and that the meso-β-scale lake-effect structure may not be sensitive to variations of ΔT within the range of observed values during lake-effect events.

The results shown in Fig. 9 indicate that given prior

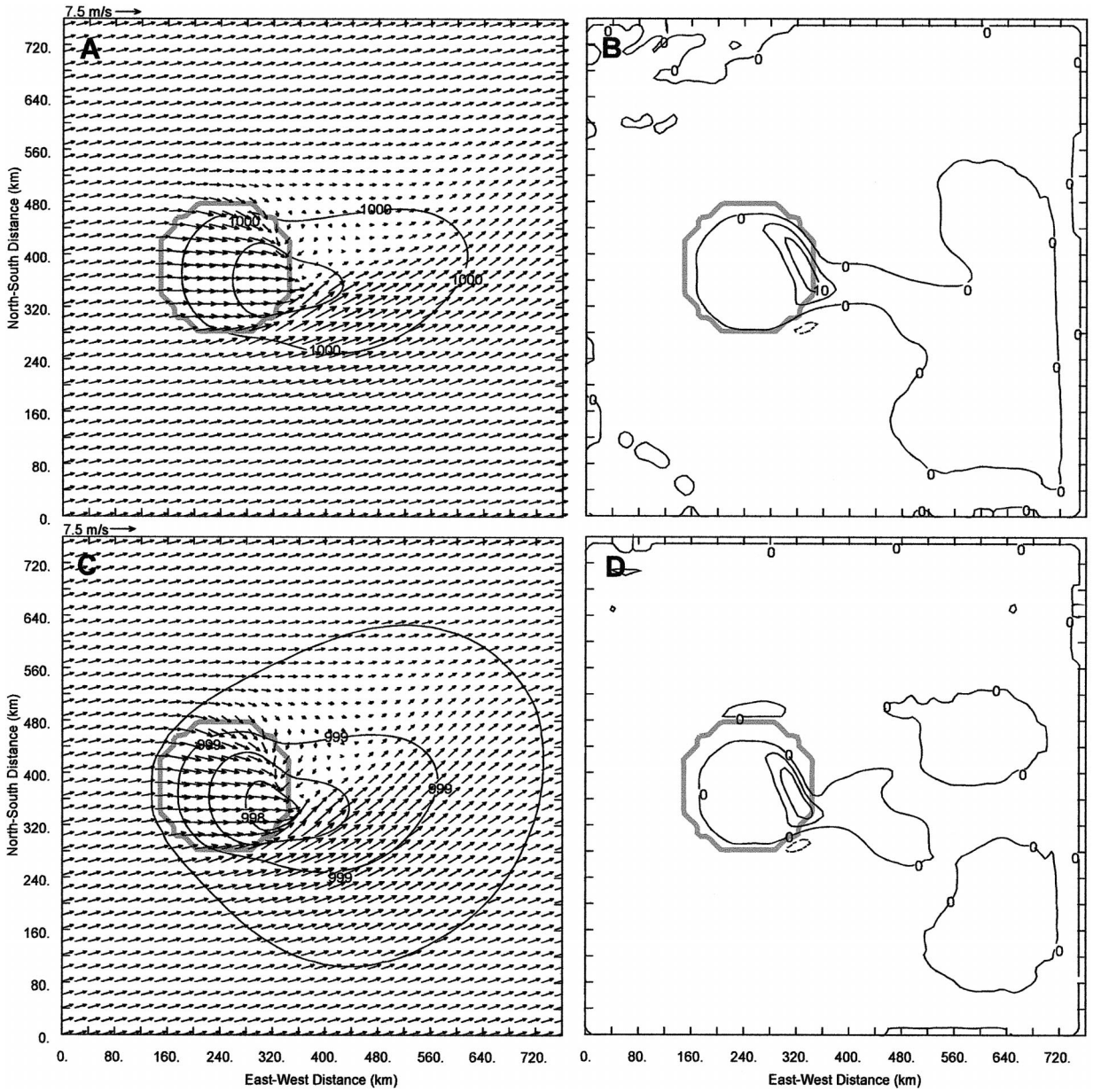

FIG. 10. The 10-m wind, surface pressure, and 1500-m vertical velocity fields for (a), (b) a shoreline band with Fr = 0.56, U/L = 0.025 m s^{-1} km^{-1}, N = 0.006 s^{-1}, and ΔT = 15.0C and (c), (d) shoreline band with Fr = 0.30, U/L = 0.025 m s^{-1} km^{-1}, N = 0.011 s^{-1}, and ΔT = 22.5C. Each simulation used U = 5.0 m s^{-1} and L = 200 km. Contour intervals of pressure and vertical velocity are 0.5 hPa and 5.0 cm s^{-1}, respectively.

knowledge of regional wind speed and direction in the vicinity of a specific lake, the lake-effect morphological regime can be determined using the ratio of wind speed to maximum fetch distance (U/L). The ratio of U/L is equivalent to the inverse of the advective residence time of an air parcel over a lake suggesting that during cold-air outbreak conditions long residence times are conducive for vortex development, intermediate residence times are favorable for shoreline bands, and short residence times are associated with widespread coverage events.

8. Discussion and conclusions

The results obtained here show that the quantity U/L effectively differentiates the three basic lake-effect morphological regimes and that the meso-β-scale lake-effect structure may not be sensitive to variations of ΔT within the range of observed values. Model simulations with low U/L values (i.e., approximately < 0.02) result in a mesoscale vortex circulation. For these cases, the vortex circulation is typically located over the lake due to the combination of the 1) hydrostatic reduction of

surface pressure in this region resulting from positive sensible heat flux over the lake and 2) differential surface diabatic and frictional forcing of the concave lakeshore curvature associated with the idealized axisymmetric lake. The development of a cyclonic mesoscale vortex can be more easily considered using a Lagrangian framework to discuss air parcels influenced by the surface heat fluxes in the vicinity of the lake. During a vortex event, the mesoscale low pressure center developing over the warm lake and the weak land-breeze winds along the shoreline cause the horizontal trajectory of the parcel to remain within the cyclonic circulation of the vortex. Therefore, a greater modification of the parcel occurs through the continual heat transfer from the lake to the parcel, and a persistent maintenance or intensification of the low pressure center over the lake occurs (Figs. 3a and 3b).

Shoreline bands (e.g., land-breeze convergence zone) were found to develop for simulation conditions with U/L values between about 0.02 and 0.09. For a given lake diameter and ΔT, the land-breeze flow opposes an increasing westerly ambient flow with increasing values of U/L. The interaction of westerly ambient flow with easterly land-breeze flow produces a wind-perpendicular convergence zone in the vicinity of the downwind shore (Figs. 3c and 3d). In a two-dimensional modeling study of the effects of large-scale flow on sea breezes, Arritt (1993) found that sea-breeze vertical motions were maximized for opposing synoptic flow of approximately 6 m s^{-1}. In a numerical study examining wind speed effects on winter lake-effect storms, Sousounis (1993) found that vertical motions associated with a convergence region near the downwind shore also had maximum amplitudes for an ambient flow of 6 m s^{-1}. Similarly, an examination of Fig. 9 shows that vertical motions were maximized for shoreline bands (i.e., intermediate values of U/L) relative to mesoscale vortex and widespread coverage events. Wind speeds resulting in shoreline band events in the current study tended to be larger than those found by both Arritt (1993) and Sousounis (1993) primarily due to greater ΔT and opposing land-breeze flow. This result suggests that an ambient wind speed most favorable for maximizing lake-effect response along a shoreline band exists for a given set of constant winter lake-effect environmental conditions.

Our results show a weak, widespread circulation over and downwind of the lake is produced at large values of U/L (>0.09). The higher wind speeds generally associated with the larger U/L simulations effectively reduce the ability of a land breeze and a wind-perpendicular convergence zone to develop along the downwind shore (Fig. 3f).

Similar to past investigations, our results indicate that the structure (i.e., morphological regime) of a winter lake-effect circulation has some dependence on Fr. Mesoscale vortex events are confined to low Froude numbers and the weak vertical motions associated with a vortex are located over the lake (Fig. 3b). A maximized lake-effect response (i.e., shoreline band) develops near the downwind shore when Froude numbers are greater than unity. For example, the greatest vertical motion for 200-km lake shoreline bands was simulated with Fr $=$ 1.4 corresponding to $U = 12.5$ m s^{-1}, $N = 0.006$ s^{-1}, and $H = 1.5$ km (Fig. 6). However, our results indicate that Fr does not uniquely differentiate morphological regimes (vortex, shoreline band, and widespread events).

While U/L effectively predicts the lake-effect mesoscale structure, note from Fig. 9 that within each morphological regime (or for a unique value of U/L) there exists a range in intensity of the mesoscale response circulation. For example, the largest variability in the maximum vertical motions occurs for shoreline band events where values range from <10 cm s^{-1} to nearly 70 cm s^{-1} for the lake-effect environments simulated. The variability of the response intensity for mesoscale vortex and widespread coverage events is smaller, with mesoscale vortex events associated with weak responses and widespread coverage events displaying moderate to weak responses. More work is needed to identify a predictive parameter of lake-effect intensity.

Although mesoscale model simulations have shown the capability of providing detailed forecasts of lake-effect systems (e.g., Ballentine et al. 1998), simpler more accessible forecasting techniques that have proven useful for operational forecasting, such as proxies, rules of thumb, and decision trees (e.g., Niziol 1987; Niziol et al. 1995), are likely to find continued use in hopes of striking some balance between the man–machine mix of the forecast process (Sousounis et al. 1999). While past mesoscale investigations have typically used the U versus ΔT parameter space to identify favorable conditions suitable for a particular mesoscale structure, the present study has identified a single quantity (U/L) that successfully predicts the lake-effect morphological regime. Therefore, a new two-dimensional parameter space could be developed for the prediction of both lake-effect structure and intensity by using U/L in combination with a quantity that describes the circulation intensity. However, it should be noted that the transitions between lake-effect morphological regimes in U/L space are not discrete, but rather zones of transition from one type of lake-effect circulation to another. In addition, results of this investigation are only applicable to cold-air outbreaks over inland water bodies in situations where important factors are differential diabatic heating and frictional convergence near the downwind shoreline.

The results of this investigation provide practical information to predict, for a circular lake, the 1) morphological regime of a mesoscale lake-effect circulation and 2) periods of transition across regimes. In real lake-effect situations lakes have complex shapes and coastlines, thus previous investigations have found wind direction to be important to the structure and prediction

APPENDIX

Model Simulation Information

Model simulations conducted. Variables included in the table are U/L, Froude number (Fr), ambient wind speed (U), lake-air temperature difference (ΔT), surface to 1.5 km stability (σ), lake diameter (L), lake-effect regime (V, vortex; B, band; W widespread), maximum vertical motion (W_{max}), spatial area of east winds, and maximum wind speed of east wind (U_{min}).

Expt	U/L (m s^{-1} km^{-1})	Fr	U (m s^{-1})	ΔT (°C)	σ (K km^{-1})	L (km)	Regime	W_{max} (cm s^{-1})	East wind ($\times$10 km^2)	U_{min} (m s^{-1})
1	0.0	0.00	0.00	22.5	1.0	200	V	3.01	2983	−2.83
2	0.0	0.00	0.00	22.5	1.0	100	V	2.69	2594	−1.91
3	0.0	0.00	0.00	22.5	1.0	300	V	2.91	3013	−3.07
4	0.005	0.11	1.00	22.5	1.0	200	V	5.10	363	−2.51
5	0.005	0.11	1.00	10.0	1.0	200	V	1.36	121	−0.66
6	0.008	0.28	2.50	22.5	1.0	300	V	9.77	344	−2.98
7	0.012	0.28	2.50	22.5	1.0	200	V	9.10	180	−2.29
8	0.016	0.56	5.00	22.5	1.0	300	B	30.08	240	−3.88
9	0.021	0.71	6.35	15.0	1.0	300	B	20.35	114	−2.59
10	0.024	0.53	4.80	16.0	1.0	200	B	14.30	61	−2.01
11	0.025	0.56	5.00	22.5	1.0	200	B	23.35	107	−3.64
12	0.025	0.28	2.50	22.5	1.0	100	B	7.12	20	−0.70
13	0.025	0.83	7.50	22.5	1.0	300	B	39.14	194	−5.13
14	0.025	0.56	5.00	7.5	1.0	200	B	5.80	3	−0.10
15	0.025	0.56	5.00	10.0	1.0	200	B	8.91	5	−0.16
16	0.025	0.56	5.00	15.0	1.0	200	B	13.65	50	−1.82
17	0.025	0.30	5.00	22.5	3.0	200	B	15.68	78	−2.90
18	0.025	0.22	5.00	22.5	6.0	200	B	9.74	56	−2.34
19	0.033	1.11	10.00	22.5	1.0	300	B	49.89	156	−5.25
20	0.038	0.83	7.50	22.5	1.0	200	B	35.81	72	−3.82
21	0.038	0.83	7.50	10.0	1.0	200	B	11.51	5	−0.10
22	0.042	1.39	12.50	22.5	1.0	300	B	66.08	122	−4.83
23	0.049	1.11	10.00	22.5	1.0	200	B	47.69	53	−3.86
24	0.049	0.56	5.00	22.5	1.0	100	B	17.07	9	−0.85
25	0.049	1.67	15.00	22.5	1.0	300	B	70.75	96	−4.83
26	0.058	0.52	11.75	19.0	6.0	200	B	13.86	4	−0.50
27	0.062	1.39	12.50	22.5	1.0	200	B	56.14	37	−4.42
28	0.074	1.67	15.00	22.5	1.0	200	B	50.30	24	−3.52
29	0.074	0.83	7.50	22.5	1.0	100	B	23.96	2	−0.09
30	0.090	2.02	18.18	10.0	1.0	200	W	9.37	0	0
31	0.090	2.02	18.18	22.5	1.0	200	W	39.20	0	0
32	0.099	1.11	10.00	22.5	1.0	100	W	27.34	0	0
33	0.109	1.22	11.00	15.0	1.0	100	W	14.46	0	0
34	0.123	1.39	12.50	22.5	1.0	100	W	29.45	0	0
35	0.148	1.67	15.00	22.5	1.0	100	W	29.68	0	0

of lake-effect storms (e.g., Hjelmfelt 1990; Hsu 1987a). Variations in lake shape and wind direction relative to the major axis of a noncircular lake will be presented in a subsequent study. In addition, the role of both topography and latent heating on lake-effect morphologies, especially near structural transition zones, requires further research.

Acknowledgments. Thanks to Dr. Mark Hjelmfelt for providing the computer code and assistance with the CSUMM. The lead author would like to thank the members of his Ph.D. thesis committee (Drs. David Kristovich, John Walsh, Robert Rauber, Mohan Ramamurthy, Mark Hjelmfelt, and Peter Sousounis) for their helpful advice, suggestions, and comments along the way to completion of this research. Thoughtful comments provided by two anonymous reviewers helped to improve the manuscript. The visible satellite image and surface weather analysis shown in Fig. 1 were provided by the Research Applications Program at the National Center for Atmospheric Research. The National Science Foundation, through Grant ATM-9816306, supported the research reported in this article. Any opinions, findings, and conclusions or recommendations expressed in this material are those of the author(s) and do not necessarily reflect the views of the National Science Foundation.

REFERENCES

Arritt, R. W., 1993: Effects of the large-scale flow on characteristic features of the sea breeze. *J. Appl. Meteor.*, **32,** 116–125.

Ballentine, R. J., A. J. Stamm, E. E. Chermack, G. P. Byrd, and D. Schleede, 1998: Mesoscale model simulation of the 4–5 January 1995 lake-effect snowstorm. *Wea. Forecasting,* **13,** 893–920.

Bauer, M. H., G. J. Mayr, I. Vergeiner, and H. Pichler, 2000: Strongly nonlinear flow over and around a three-dimensional mountain as a function of the horizontal aspect ratio. *J. Atmos. Sci.,* **57,** 3971–3991.

Biggs, W. G., and M. E. Graves, 1962: A lake breeze index. *J. Appl. Meteor.,* **1,** 474–480.
Braham, R. R., Jr., 1983: The Midwest snow storm of 8–11 December 1977. *Mon. Wea. Rev.,* **111,** 253–272.
——, and R. D. Kelly, 1982: Lake-effect snow storms on Lake Michigan, USA. *Cloud Dynamics,* E. Agee and T. Asai, Eds., D. Reidel, 87–101.
Buckingham, E., 1914: On physically similar systems: Illustrations of the use of dimensional equations. *Phys. Rev.,* **4,** 345–376.
Businger, J. A., J. C. Wyngaard, Y. Izumi, and E. F. Bradley, 1971: Flux-profile relationships in the atmospheric surface layer. *J. Atmos. Sci.,* **28,** 181–189.
Chang, S. S., and R. R. Braham Jr., 1991: Observational study of a convective internal boundary layer over Lake Michigan. *J. Atmos. Sci.,* **48,** 2265–2279.
Cooper, K. A., M. R. Hjelmfelt, R. G. Derickson, D. A. R. Kristovich, and N. F. Laird, 2000: Numerical simulations of transitions in boundary layer convective structures in a lake-effect snow event. *Mon. Wea. Rev.,* **128,** 3283–3295.
Forbes, G. S., and J. M. Merritt, 1984: Mesoscale vortices over the Great Lakes in wintertime. *Mon. Wea. Rev.,* **112,** 377–381.
Grossman, R. L., 1982: An analysis of vertical velocity spectra obtained in the BOMEX fair-weather, trade-wind boundary layer. *Bound.-Layer Meteor.,* **23,** 323–357.
Hjelmfelt, M. R., 1990: Numerical study of the influence of environmental conditions on lake-effect snowstorms on Lake Michigan. *Mon. Wea. Rev.,* **118,** 138–150.
——, and R. R. Braham Jr., 1983: Numerical simulation of the airflow over Lake Michigan for a major lake-effect snow event. *Mon. Wea. Rev.,* **111,** 205–219.
Hsu, H.-M., 1987a: Mesoscale lake-effect snowstorms in the vicinity of Lake Michigan: Linear theory and numerical simulations. *J. Atmos. Sci.,* **44,** 1019–1040.
——, 1987b: Study of linear steady atmospheric flow above a finite surface heating. *J. Atmos. Sci.,* **44,** 186–199.
Kelly, R. D., 1984: Horizontal roll and boundary-layer interrelationships observed over Lake Michigan. *J. Atmos. Sci.,* **41,** 1816–1826.
——, 1986: Mesoscale frequencies and seasonal snowfalls for different types of Lake Michigan snowstorms. *J. Climate Appl. Meteor.,* **25,** 308–321.
Klemp, J. B., and D. R. Durran, 1983: An upper boundary condition permitting internal gravity wave radiation in numerical mesoscale models. *Mon. Wea. Rev.,* **111,** 430–444.
Kristovich, D. A. R., 1993: Mean circulations of boundary-layer rolls in lake-effect snow storms. *Bound.-Layer Meteor.,* **63,** 293–315.
——, and N. F. Laird, 1998: Observations of widespread lake-effect cloudiness: Influences of lake surface temperature and upwind conditions. *Wea. Forecasting,* **13,** 811–821.
Kundu, P. K., 1990: *Fluid Mechanics.* Academic Press, 638 pp.
Laird, N. F., 1999: Observation of coexisting mesoscale lake-effect vortices over the western Great Lakes. *Mon. Wea. Rev.,* **127,** 1137–1141.
——, 2001: Simulations of winter mesoscale circulations associated with an isolated lake. Ph.D. dissertation, University of Illinois, 146 pp. [Available from University Microfilms Inc., P.O. Box 1346, Ann Arbor, MI 48106.]
Lin, Y.-L., 1986: Calculation of airflow over an isolated heat source with application to the dynamics of V-shaped clouds. *J. Atmos. Sci.,* **43,** 2736–2751.
——, 1989: Inertial and frictional effects on stratified hydrostatic airflow past an isolated heat source. *J. Atmos. Sci.,* **46,** 921–936.
——, and R. B. Smith, 1986: Transient dynamics of airflow near a local heat source. *J. Atmos. Sci.,* **43,** 40–49.
Mahrer, Y., and R. A. Pielke, 1977: A numerical study of the airflow over irregular terrain. *Contrib. Atmos. Phys.,* **50,** 98–113.
——, and ——, 1978: A test of an upstream spline interpolation technique for the advective terms in a numerical mesoscale model. *Mon. Wea. Rev.,* **106,** 818–830.
Niziol, T. A., 1987: Operational forecasting of lake effect snowfall in western and central New York. *Wea. Forecasting,* **2,** 310–321.
——, W. R. Snyder, and J. S. Waldstreicher, 1995: Winter weather forecasting throughout the eastern United States. Part IV: Lake effect snow. *Wea. Forecasting,* **10,** 61–77.
Passarelli, R. E., Jr., and R. R. Braham Jr., 1981: The role of the winter land breeze in the formation of Great Lake snow storms. *Bull. Amer. Meteor. Soc.,* **62,** 482–491.
Pease, S. R., W. A. Lyons, C. S. Keen, and M. R. Hjelmfelt, 1988: Mesoscale spiral vortex embedded within a Lake Michigan snow squall band: High resolution satellite observations and numerical model simulations. *Mon. Wea. Rev.,* **116,** 1374–1380.
Pielke, R. A., 1974: A three-dimensional numerical model of the sea breezes over south Florida. *Mon. Wea. Rev.,* **102,** 115–139.
——, 1984: *Mesoscale Meteorological Modeling.* Academic Press, 599 pp.
Pitts, D. E., J. T. Lee, J. Fein, Y Sasaki, K. Wagner, and R. Johnson, 1977: Mesoscale cloud features observed from Skylab. *Skylab Explores the Earth,* NASA-SP-80, NASA Scientific and Technical Information Office, Huntsville, AL, 479–501.
Priestley, C. H. B., 1957: Convection from the earth's surface. *Proc. Roy. Soc. London,* **A238,** 287–304.
Rose, B. L., 2000: The role of upstream lakes in determining downstream severe lake-effect snowstorms. Ph.D. dissertation, University of Illinois, 183 pp. [Available from University Microfilms Inc., P.O. Box 1346, Ann Arbor, MI 48106.]
Schoenberger, L. M., 1986: Mesoscale features of the Michigan land breeze using PAM II temperature data. *Wea. Forecasting,* **1,** 127–135.
Segal, M., and R. W. Arritt, 1992: Nonclassical mesoscale circulations caused by surface sensible heat-flux gradients. *Bull. Amer. Meteor. Soc.,* **73,** 1593–1604.
Smith, R. B., 1988: Linear theory of stratified flow past an isolated mountain in isosteric coordinates. *J. Atmos. Sci.,* **45,** 3889–3896.
——, and V. Grubisic, 1993: Aerial observations of Hawaii's wake. *J. Atmos. Sci.,* **50,** 3728–3750.
Sousounis, P. J., 1993: A numerical investigation of wind speed effects on lake-effect storms. *Bound.-Layer Meteor.,* **64,** 261–290.
——, and H. N. Shirer, 1992: Lake aggregate mesoscale disturbances. Part I: Linear analysis. *J. Atmos. Sci.,* **49,** 80–96.
——, G. E. Mann, G. S. Young, R. B. Wagenmaker, B. D. Hoggatt, and W. J. Badini, 1999: Forecasting during the Lake-ICE/SNOWBANDS field experiments. *Wea. Forecasting,* **14,** 955–975.
Stull, R. B., 1988: *An Introduction to Boundary Layer Meteorology.* Kluwer Academic, 669 pp.
Ulrickson, B. L., and C. F. Mass, 1990: Numerical investigation of mesoscale circulations over the Los Angeles Basin. Part I: A verification study. *Mon. Wea. Rev.,* **118,** 2138–2161.
Vignaux, G. A., 1986: Dimensional analysis in operations research. *N. Z. Operations Res.,* **14,** 81–92.
Walsh, J. E., 1974: Sea breeze theory and applications. *J. Atmos. Sci.,* **31,** 2012–2026.
Woodcock, A. H., 1940: Convection and soaring over the open sea. *J. Mar. Res.,* **3,** 248–253.
Xie, L., and Y.-L. Lin, 1996: A numerical study of stratified airflow over mesoscale heat sources with application to Carolina coastal frontogenesis. *Mon. Wea. Rev.,* **124,** 2807–2827.